ACS APPLIED MATERIALS & INTERFACES

Research Article

www.acsami.org

Mesoporous TiO_2 Spheres Interconnected by Multiwalled Carbon Nanotubes as an Anode for High-Performance Lithium Ion Batteries

Nguyen Thi Hong Trang,[†,§] Zahid Ali,[†,‡,§] and Dae Joon Kang*[,†]

[†]Department of Physics, Sungkyunkwan University, Suwon 440-746, Republic of Korea

[‡]National Institute of Lasers and Optronics, P.O. Nilore, 45650 Islamabad, Pakistan

Supporting Information

ABSTRACT: We report on the excellent electrochemical response of lithium ion batteries that use a composite material comprised of mesoporous titanium dioxide (MTO) spheres and multiwalled carbon nanotubes (MWCNTs) for the anode. The composite structure was synthesized via a combined sol–gel and solvothermal method, and the batteries exhibited unprecedented discharge capacity, cycling stability, and reversibility when compared to those based on commercially available TiO_2 nanopowders and mesoporous TiO_2 spheres. The inclusion of the composite structure resulted in an improvement in electronic and ionic conductivity, a larger surface area, and a colossal number of open channels in the synthesized structure that allowed for lithium ion intercalation. We achieved a Coulombic efficiency of nearly 100% and a discharge capacity as high as 316 mA h g^{-1} at a rate of C/5, which is 1.9 times higher than that which is practically attainable with TiO_2. Moreover, we observed a capacity loss of only 3.1% after 100 cycles, which indicates that the synthesized structure has a highly stable nature.

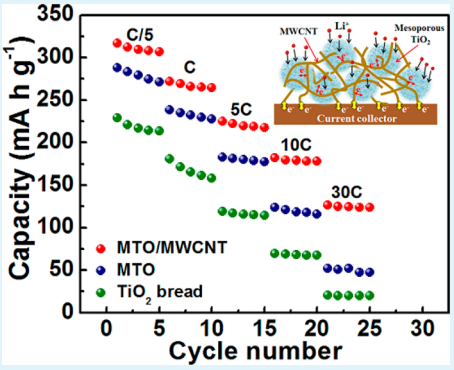

KEYWORDS: *mesoporous TiO_2, multiwalled carbon nanotube, lithium ion batteries, sol–gel, solvothermal*

1. INTRODUCTION

A major challenge that limits the practical use of lithium (Li) ion batteries in high-power electric vehicles and portable electronic devices is that new materials with a high energy density, long cycle life, and excellent rate capability should be developed.[1−4] Materials based on titanium dioxide (TiO_2) have been recently proposed as promising alternatives to traditional carbonaceous anodes due to their low cost, environmental friendliness, improved safety, higher structural stability, and high rate performance.[5−7] TiO_2 has various rutile, anatase, and brookite allotropes, and of these, anatase-phase TiO_2 has been extensively studied because it can reversibly intake 0.5 Li ions per formula unit through an electrochemical reaction path that connects octahedral interstitial sites, following the equation $TiO_2 + xLi + xe^- = Li_xTiO_2$ and, thus, delivering a theoretical capacity of 330 mA hg^{-1}. However, strong repulsive forces generally hinder Li ion insertion in TiO_2, and hence, the practically attainable capacity is only 168 $mAhg^{-1}$.[8,9] A relatively high Li ion insertion/extraction potential (versus Li^+/Li) at 1.7 V for anatase TiO_2 does not overlap with the Li electroplating potential and inhibits the common growth of Li dendrites on the surface of the TiO_2 anode, ensuring a longer cell life. Furthermore, a small change in volume (less than 4%) during the Li insertion/extraction process leads to an enhanced structural stability and a prolonged cycle life.[6] However, technical obstacles impede the further development of anode materials based on anatase TiO_2, such as their relatively low ionic and electronic conductivities and limited specific capacity.

In recent years, nanostructured TiO_2 materials with a reduced ion diffusion length have been proposed in order to improve the low ionic conductivity, but such efforts have not been successful so far.[10−13] Unfortunately, the methods that have been attempted still suffer from technical issues, including the aggregation of the nanopowders, poor electrical conductivity, and low particle-packing density. Recently, micrometer-sized mesoporous materials, such as $LiFePO_4$ and TiO_2, have shown the potential to address the aforementioned problems while still providing the advantages of the nanomaterials.[12,14−17] Mesoporous materials are attractive hosts for Li intercalation because they possess a large surface area that provides more open channels for Li ion insertion/extraction. Moreover, the thin walls of these mesoporous materials reduce the diffusion length of the Li ion in the solid phase, and their pores allow the electrolyte ions to flow smoothly. The optimal morphology of these micrometer-sized materials is considered to be spherical because microspheres provide a high packing density due to better particle mobility, resulting in a more compact electrode layer for use with conventional electrode fabrication technology.[12,18] The compact layer helps to attain high volumetric energy and power density as well as uniform electrode layers. In addition, the electronic conductivity of the TiO_2-based electrodes can be improved by synthesizing composites that incorporate a conductive matrix,[19−25] and

Received: November 20, 2014
Accepted: January 29, 2015
Published: January 29, 2015

DOI: 10.1021/am508158v
ACS Appl. Mater. Interfaces 2015, 7, 3676−3683

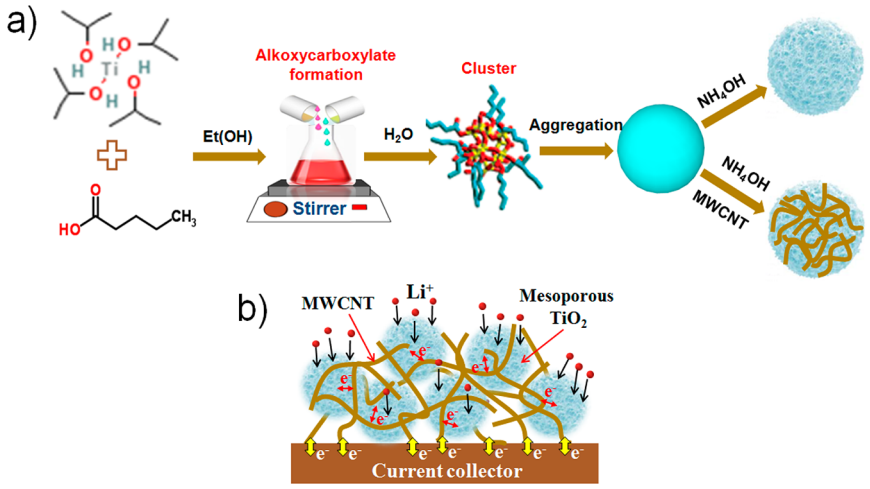

Figure 1. (a) Schematic of the two-stage synthesis of the MTO/MWCNT composite. (b) Schematic of Li^+ insertion/desertion reaction and electron transport process in the MTO/MWCNT composite.

among the various conductive materials that are available in the fields of energy conversion and storage, carbon nanotubes (CNTs) have been extensively investigated because they possess a high electronic conductivity and high mechanical strength.[20,26,27]

Although numerous approaches have been proposed for synthesizing TiO_2/MWCNT composites, no report on the synthesis of composites with a mesoporous structure composed of anatase TiO_2 and MWCNTs suitable for a high performance lithium-ion battery is available. Most reports thus far were about as-grown TiO_2 on CNT, which is difficult for TiO_2 to directly nucleate and grow on the surface of pristine CNTs, thus leading to serious degradation of the pristine properties of CNTs during the synthesis.[28−30] In addition, there were some reports on the decorated TiO_2 on CNTs by inducing aggregation of TiO_2 nanoparticles on the CNT surface[31,32] and simple composites composed of TiO_2 nanoparticles and CNTs without mesoporosity.[20,21] Such composites resulted in low structural stability during charge/discharge processes, low lithium storage capacity, and poor rate performance.

We propose a new approach that involves a facile synthetic route to synthesize a mesoporous TiO_2 sphere/multiwalled carbon nanotube (MTO/MWCNT) composite via a combined sol−gel and solvothermal method. Long and tortuous CNTs bridge the adjacent mesoporous TiO_2 spheres that not only facilitate electron transfer but also inhibit the aggregation of the spheres, resulting in a high contact area between the electrode and electrolyte. Hence, the synthetic structure transports electrolyte ions and electrons into the inner regions of the electrode. Our proposed architecture provides highly reversible capacities and exhibits a significant improvement in the cyclic performance. We also demonstrate that the Li intercalation capacity of the MTO/MWCNT composite at high charge−discharge rates increases dramatically as compared to that of mesoporous TiO_2 and to other TiO_2/CNT composites.

2. EXPERIMENTS

2.1. Materials. Titanium(IV) isopropoxide (TTIP, 97%), valeric acid (99%), absolute ethanol (99.9%), benzyl alcohol (BA, 99,5%), and ammonium hydroxide (NH_4OH, 28%) were purchased from Sigma-Aldrich, Korea. MWCNTs (40 nm in diameter and several tens of microns in length and acid functionalized in a water solution) were purchased from Nanokarbon Co., Korea. All chemicals were used as received without further purification.

2.2. Synthesis. The MTO/MWCNT composites were synthesized in two steps via a combined sol−gel and solvothermal method, as shown in Figure 1a. First, the TiO_2 spheres were synthesized following instructions from prior literature.[33] A typical reaction was performed where 0.4 mL of valeric acid was added into 20 mL of ethanol, followed by the addition of 0.3 mL (1 mmol) of TTIP. The solution was then stirred vigorously and was heated at 80 °C for 6 h under reflux in the air. Next, hydrolysis and condensation were initiated by adding 11 mL of a solution consisting of 1 mL of deionized (DI) water and 10 mL of ethanol in order to cause the particles to gradually precipitate, resulting in a turbid solution for 4 h. The precipitate was recovered by centrifuging and decanting the liquid and was then washed several times with ethanol and DI water.

In the second step, the washed TiO_2 spheres were dispersed in a 13 mL solution consisting of 3 mL of DI water and 10 mL of ethanol, and then CNTs were added at a TiO_2 to CNTs weight ratio of 4:1 with 1 mL of NH_4OH (28%, Aldrich). Then, 2 mL of benzyl alcohol (BA) was added as a surfactant. The solution was vigorously stirred for 1 h, sealed in a Teflon-lined autoclave, and placed in a furnace at 160 °C for 16 h to remove the carbon species. The obtained material was filtered, washed twice in ethanol, and dried in an oven at 90 °C overnight, followed by annealing of as-synthesized TiO_2 spheres in an argon atmosphere at 400 °C for 2 h to produce the MTO/MWCNT composites. The mesoporous TiO_2 was synthesized in the same manner as the composite structure, except that the carbon nanotubes and the benzyl alcohol were not added.

2.3. Characterization. *Physical Characterization.* The crystal structure and purity of the samples were studied via X-ray diffraction (XRD, D8 FOCUS 2200 V, Bruker AXS) using Cu Kα radiation (λ = 1.5418 Å) and Raman spectroscopy (Renishaw RM 1000−Invia). The morphology of the samples was then examined using a field emission scanning electron microscope (FE-SEM, JEOL JSM−7401F). Measurements of the nitrogen adsorption−desorption isotherms of the materials were carried out at 77 K using a Digisorb 2006 instrument (Micrometrics, Shimadzu) to estimate the surface area and the pore size.

Electrochemical Characterization. The anodes of the lithium ion batteries were prepared by using either a mixture of the active material (MTO/MWCNT composite structure) with polyvinylidene difluoride (PVDF) as a binder (weight ratio of 90:10) or active material (approximately 30 nm anatase commercial TiO_2 or MTO), carbon black, and PVDF at a weight ratio of 80:10:10. These ingredients were added in an *N*-methyl-2-pyrrolidone solution to prepare the slurry that was then coated onto a copper foil and dried overnight at 110 °C to ensure solvent evaporation. 2032-type coin cells were assembled in an argon-filled glovebox using $LiPF_6$ as an electrolyte and lithium foil as

DOI: 10.1021/am508158v
ACS Appl. Mater. Interfaces 2015, 7, 3676−3683

the counter electrode. The electrolyte solution was composed of 1 M $LiPF_6$ dissolved in a mixture of ethylene carbonate (EC) and dimethyl carbonate (DMC) at a volume ratio of EC/DMC = 1:1. Cyclic voltammograms (CVs) were carried out with three-electrode cells and were recorded from 3.0 to 0 V at a scan rate of 0.1 mV s^{-1} using a CHI 600 electrochemical station (CHI Inc., Austin, TX, USA). Charge–discharge tests were performed using a battery tester (TOSCAT-3000U, Toyo System, USA), and electrochemical impedance spectroscopy (EIS) measurements were performed with an open-circuit voltage state of fresh cells using a CHI600 electrochemical workstation (Shanghai Chenhua Instrument Ltd., China). The frequency of the EIS measurements ranged from 0.01 Hz to 100 kHz.

3. RESULTS AND DISCUSSION

Figure 1a shows a schematic of the two-stage synthesis process. Titanium alkoxycarboxylate was first formed by adding valeric acid to the TTIP solution. The small clusters were produced through the hydrolysis and condensation of the alkoxycarboxylate after the addition of water, leading to the formation of a composite microsphere consisting of TiO_2 and carbon species. In the next stage, a solvothermal reaction with NH_4OH for 16 h at 160 °C resulted in the removal of the carbon species, resulting in TiO_2 based mesoporous microspheres. Benzyl alcohol (BA) was used as the surfactant, and the phenyl ring of the BA attached to the graphitic surfaces of the CNTs via $\pi-\pi$ stacking. Then, the hydroxyl groups of the BA interacted directly with the precursors in the solvothermal process as linkers,[34] leading to the formation of a mesoporous TiO_2/MWCNT composite structure.

The XRD spectra (Figure 2) reveal that after annealing in argon at 400 °C, the TiO_2 spheres synthesized by this route

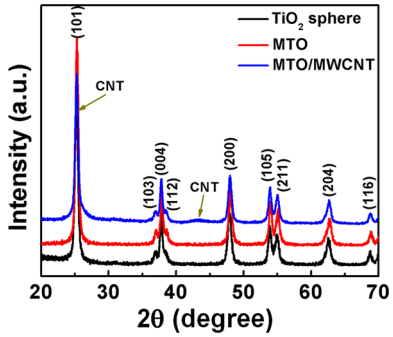

Figure 2. XRD patterns of TiO_2 spheres, mesoporous TiO_2 spheres, and MTO/MWCNT composite.

exhibited good crystallinity and typical anatase structures, as indicated in the JCPDS card 21-1272. After the solvothermal treatment with NH_4OH, the as-prepared mesoporous TiO_2 retained the same diffraction pattern as TiO_2. Anatase peaks also appeared in the composites together with the typical (002) and (100) peaks of CNT, and these observations are consistent with previous results.[35] No peaks resulting from the presence of impurities were observed in the XRD patterns, indicating the absence of competing phases of TiO_2. The small characteristic diffraction peaks of the CNTs were probably a result of the small amount of CNTs in the composites.

Raman spectroscopy was also performed in order to investigate the crystal structures of the TiO_2 and the MWCNTs in the mesoporous composites. As shown in Figure 3, four vibrational modes with strong intensities at 142 (E_g), 396 (B_{1g}), 517 (A_{1g}), and 639 cm^{-1} (E_g) were observed in the Raman spectra of the TiO_2 spheres and of the mesoporous TiO_2 spheres (Figure 3a), and these results are consistent with those reported for anatase TiO_2 in the literature.[21] These peaks also appear in the MTO/MWCNT composite (Figure 3b), although shifted toward higher frequencies, and such changes can be reasonably attributed to the interaction between TiO_2 and CNTs.[36] Furthermore, two characteristic peaks appeared in the composite spectrum at wavelengths of approximately 1353 and 1586 cm^{-1}, which correspond to the disordered carbon (D band) and graphitic carbon (G band) of the CNTs, respectively. A higher G band/D band ratio clearly indicates the absence of either amorphous carbon or impurities in the MTO/MWCNT composites. The CNTs did not exhibit a disordered structure after the solvothermal treatment used to form a composite with the mesoporous TiO_2. The content of MWCNT in the composite was determined by thermogravimetric analysis in the air with a heating rate of 10 °C/min, indicating an optimum content of 20 wt % MWCNT (see Supporting Information Figure S1)

Figure 4 shows FE-SEM images that exhibit the morphologies of the TiO_2 spheres, mesoporous TiO_2 spheres, and MTO/MWCNT composites. The FE-SEM images (Figures 4a,d) reveal that the TiO_2 spheres were almost spherical in shape, with a typical diameter of 600 nm. Unlike the as-synthesized TiO_2 spheres, which have an almost smooth surface (Figure 4a), it is evident in Figure 4b and e that after treatment with NH_4OH through the solvothermal reaction, the microspheres transformed into mesoporous structures with a rough surface containing granular features of ~30 nm in diameter. The inset of Figure 4e and TEM images in Figure S2 reveal that the sub-micron-sized spheres were composed of a porous network of nanoparticles with multiple contacts with neighboring nanoparticles. Figure 4c and f clearly show that

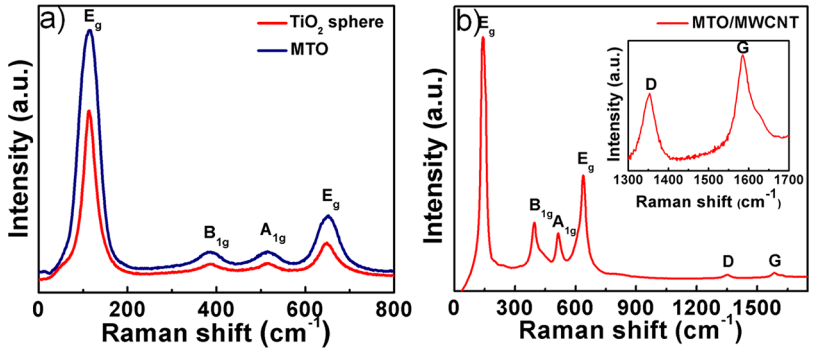

Figure 3. Raman spectra of (a) TiO_2 spheres, mesoporous TiO_2 spheres, and (b) MTO/MWCNT composites.

DOI: 10.1021/am508158v
ACS Appl. Mater. Interfaces 2015, 7, 3676–3683

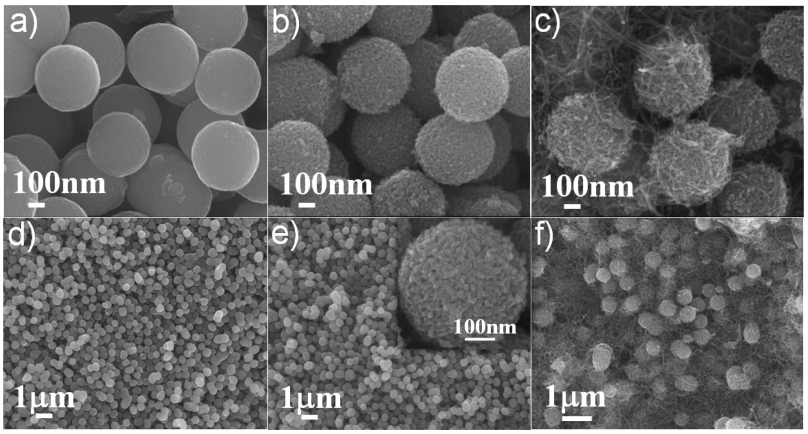

Figure 4. FE-SEM images of (a, d) TiO_2 spheres, (b, e) mesoporous TiO_2 spheres, and (c, f) MTO/MWCNT composite.

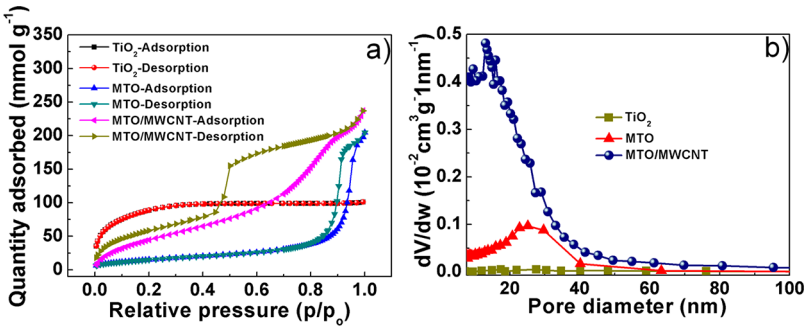

Figure 5. (a) Nitrogen sorption isotherms for commercial TiO_2 nanopowders, mesoporous TiO_2 (MTO) spheres, and MTO/MWCNT. (b) The pore size distributions for respective samples.

the MWCNTs were dispersed uniformly between the mesoporous TiO_2 spheres, and that the MWCNTs acted as bridge to effectively separate the spheres from one another, leading to a porous architecture with a large specific surface area. Moreover, the CNTs served as conducting wires, connecting mesoporous TiO_2 spheres in order to form an interconnected network that could further improve the conductivity and stability of the composite and greatly enhance the storage capacity of the lithium ion devices.

The specific surface area and the porosity of the prepared samples were determined by using the Brunauer–Emmett–Teller (BET) method to measure the nitrogen isothermal adsorption–desorption. The samples were degassed at 200 °C for 15 h before the gas sorption measurements. As shown in Figure 5a, a type I isotherm was obtained, suggesting the TiO_2 spheres had a microporous nature. The distinct hysteresis loops for the mesoporous TiO_2 spheres (H1 loop) and MTO/MWCNT composite samples (H_2 loop) can be attributed to a type IV isotherm, which is associated with capillary condensation in the mesoporous materials according to classification of the *International Union of Pure and Applied Chemistry*.[37]

As shown in Table 1, the surface area of the TiO_2 spheres increased from 42 to 121 $m^2\ g^{-1}$, and the pore volume increased from 0.052 to 0.185 $cm^3\ g^{-1}$ after the solvothermal treatment with NH_4OH, forming a mesoporous structure. After introducing the CNTs, the resulting three-dimensional (3-D) MTO/MWCNT composite exhibited a higher specific surface area (144 $m^2\ g^{-1}$) and a larger pore volume (0.197 $cm^3\ g^{-1}$) due to the high packing density of the rigid MWCNTs intertwined with the MTO spheres. These MWCNTs

Table 1. BET Surface Area and Porosity of the Prepared Materials

sample	BET surface area (m^2g^{-1})	pore volume (cm^3g^{-1})	pore size (nm)
TiO_2 spheres	42	0.052	1–2
MTO spheres	121	0.185	29–35
MTO/MWCNT	144	0.197	17–25

effectively prevented the TiO_2 spheres from stacking and uniformly filled the free space between the MTO spheres. The pore-size distributions were plotted by using the Barrett–Joyner–Halenda (BJH) method, as shown in Figure 5b. The BJH equation indicated that the pore size of the MTO/MWCNT composite was approximately 17–25 nm, which is smaller than that of mesoporous TiO_2 spheres (29–35 nm). The narrow distribution of the pore size is consistent with an H1-type hysteresis loop, indicating that uniform mesoporous TiO_2 spheres were obtained using this simple method. The relatively large surface area provided by the MTO/MWCNT composites increased the electrolyte/electrode contact area and produced more channels for Li ion insertion/extraction, resulting in a higher specific capacity.

The MTO/MWCNT composite material was evaluated for use as an anode for LIBs by investigating its electrochemical response, including its cyclic voltammogram behavior, galvanostatic charge/discharge measurements, and electrochemical impedance spectroscopy (EIS). The results provided the key parameters of the device performance, including the specific capacity, charge transport properties, rate capability, and stability.

DOI: 10.1021/am508158v
ACS Appl. Mater. Interfaces 2015, 7, 3676–3683

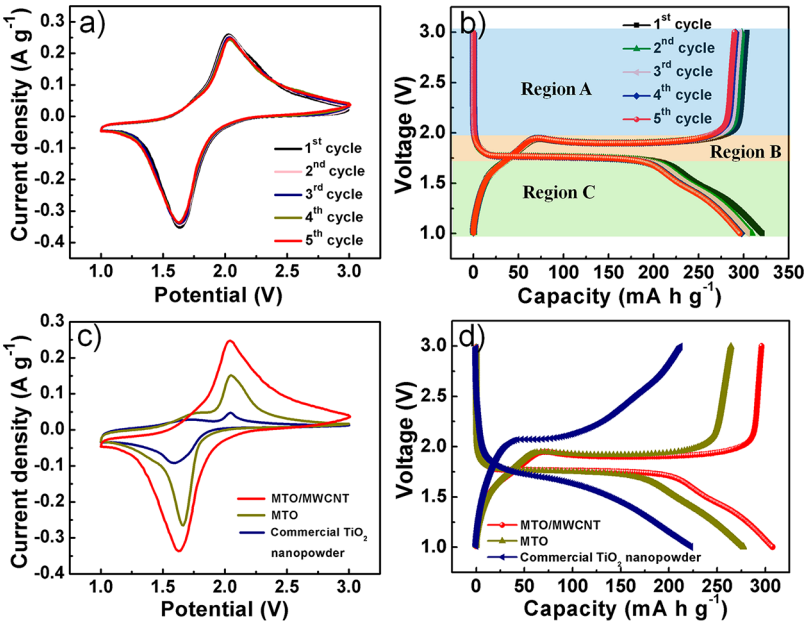

Figure 6. (a) Cyclic voltammograms of the MTO/MWCNT composite at a scan rate of 0.1 mV s^{-1} for the first five cycles. (b) Charge/discharge voltage profiles of the MTO/MWCNT composite at a current rate of C/5 for the first five cycles. (c) Cyclic voltammograms at a scan rate of 0.1 mV s^{-1} and (d) charge/discharge voltage profiles at a current rate of C/5 for the TiO_2 spheres, mesoporous TiO_2 spheres, and MTO/MWCNT composite.

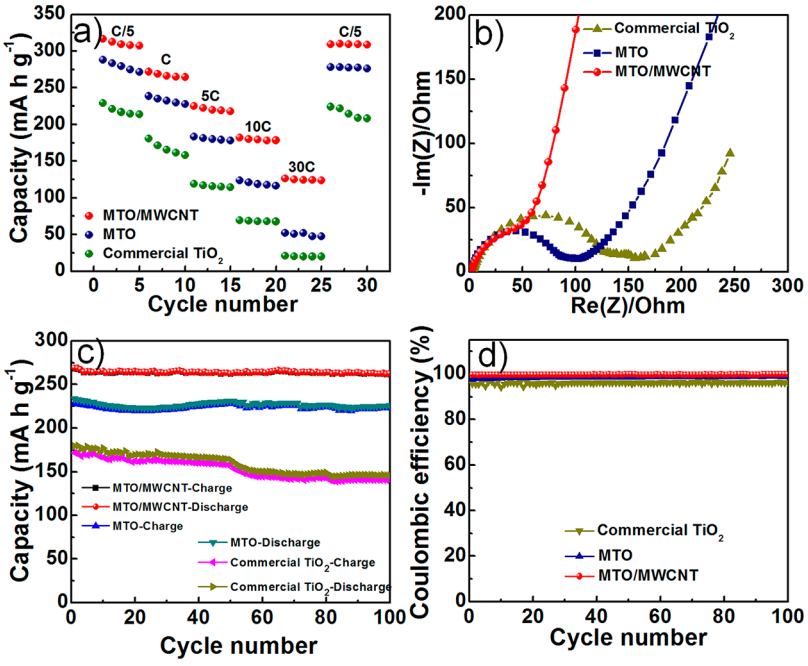

Figure 7. (a) Rate capability of TiO_2 spheres, mesoporous TiO_2 spheres, and MTO/MWCNT composite. (b) Nyquist plots for TiO_2 spheres, mesoporous TiO_2 spheres, and MTO/MWCNT composite. (c) Cycling performance and (d) Coulombic efficiency of TiO_2 spheres, mesoporous TiO_2 spheres, and MTO/MWCNT composite up to 100 cycles at a 1C charge−discharge rate.

Figure 6a shows the cyclic voltammograms of the MTO/MWCNT anode for the first five scans at a scan rate of 0.1 mV s^{-1}. The anode exhibited well-defined redox peaks at approximately 1.61 V (cathodic) and 2.03 V (anodic), demonstrating an ideal electrochemical behavior resulting from the Li^+ insertion/extraction into/out of the anatase TiO_2. Generally, anatase TiO_2 shows a pair of redox peaks in the voltage range from 1.73 to 1.98 V.[38] However, the redox peaks for the MTO/MWCNT composite shifted slightly toward the cathode potential as compared to commercial TiO_2 and mesoporous TiO_2 (Figure 6c). This shift could be attributed to the presence of the MWCNTs and the interconnection between the mesoporous TiO_2 and the MWCNTs. It is worth noting that the CV curve showed a slightly distorted rectangular shape, a typical characteristic of charging/discharging behavior originating from the TiO_2 and CNTs. Furthermore, these peaks showed almost no change in the amplitude or the voltage during the subsequent cycles,

DOI: 10.1021/am508158v
ACS Appl. Mater. Interfaces 2015, 7, 3676−3683

indicating good stability and a high reversibility for the MTO/MWCNT composite-based electrodes. In contrast, the changes in the CV shape in the first cycle of the commercial TiO_2 and of the mesoporous TiO_2 (see Supporting Information, Figure S3a,b) might correspond to an irreversible loss in capacity. The gradual increase in intensity for both the cathodic and the anodic peaks suggests the presence of a possible activation process and/or trapping of fewer Li^+ ions during the subsequent cycles, which was confirmed by the corresponding charge/discharge voltage profiles (see Supporting Information, Figure S3c,d).

Figure 6b shows the charge/discharge voltage profiles of the MTO/MWCNT composite at a current rate of C/5 for the first five cycles. Three distinct regions can be observed in the voltage profiles of the composite during the discharge process. Region A ranges from the open circuit voltage to 1.75 V and shows a rapid voltage drop as a result of the homogeneous Li^+ insertion into the bulk by a solid-solution insertion mechanism.[39] The well-known two-phase plateau is observed in region B at 1.75 V, where Li-rich and Li-poor phases coexist. The plateaus are related to the phase transition between the tetragonal and orthorhombic phases associated with the Li ion insertion into anatase TiO_2.[6,23] After the two-phase plateau, region C (below 1.75 V) exhibits a descending behavior that can be ascribed to the reversible surface/interface lithium storage on the TiO_2 spheres and MWCNTs.[38] The shape and magnitude of the first five charge/discharge cycles remained almost the same due to the good stability of the composite structure, which is in good agreement with the CV curves shown in Figure 6a. The improvement in the stability may be attributed to the intimate networking between the mesoporous TiO_2 spheres via MWCNTs; hence Li^+ ions are easily diffused into and out of the TiO_2 spheres without being trapped in the anatase framework. Furthermore, the MTO/MWCNT composites showed extended plateaus when compared with commercial TiO_2 and mesoporous TiO_2 spheres (Figure 6d). The cyclic voltammetry measurements confirmed that the MTO/MWCNT composite showed a larger redox current than commercial TiO_2 or mesoporous TiO_2 spheres (Figure 6c). These results indicate that the MTO/MWCNT composite provides a better charge−discharge capacity.

The effectiveness of the unique structure of the MTO/MWCNT composite toward improving the rate capacity was demonstrated by comparing the rate performances of the MTO/MWCNT composite, mesoporous TiO_2 spheres, and commercial TiO_2 at current rates of C/5, C, 5C, 10C, and 30C (Figure 7a). The introduction of conductive MWCNTs into MTO spheres formed a 3-D hierarchical structure, and the MTO/MWCNT mesoporous structures exhibited the highest rate capacity among the three samples. A discharge capacity as high as 316 mA h g^{-1} was delivered at a rate of C/5, which is higher than the best values that have been reported so far for TiO_2-based anode materials for LIBs, including mesoporous TiO_2(B) (230 mA h g^{-1}),[17] mesoporous anatase TiO_2 (280 mA h g^{-1}),[40] TiO_2−graphene−CNT nanocomposites (200 mA h g^{-1}),[41] graphene-wrapped TiO_2 hollow structures (175 mA h g^{-1}),[23] and graphene−TiO_2 nanosheets (210 mA h g^{-1}).[42]

At higher discharge/charge rates, the difference between the capacities of the MTO/MWCNT-based cells and commercial TiO_2 and MTO cells was more prominent due to the high conductivity and high surface area offered by the novel hybrid mesoporous structure of the MTO/MWCNT composites. The capacity retention was found to be of approximately 270 mA h g^{-1}, 222 mA h g^{-1}, 180 mA h g^{-1}, and 125 mA h g^{-1} at current rates of 1C, 5C, 10C, and 30C, respectively. More importantly, a stable capacity of 300 mA h g^{-1} was obtained even when the rate was reduced back to C/5, suggesting good structural stability and high reversibility even after a high charge−discharge rate. It is noteworthy that the capacity obtained by the MTO/MWCNT composite at a rate of 30C (125 mA h g^{-1}) was higher than that obtained at a rate of 5C for commercial TiO_2 (117 mA h g^{-1}) and 10C for the mesoporous TiO_2 (119 mA h g^{-1}). The higher capacity retention at higher current rates clearly indicates a better rate capability for the MTO/MWCNT composite. The improved electrochemical properties are believed to be a result of the unique structure of the composite; that is, the CNT interconnection and the porous structure provide rapid transport of electrons and lithium ions and also facilitates the exchange of electrons and lithium ions at the mesoporous TiO_2/electrolyte interface, as shown in Figure 1b.

To investigate the electrochemical properties upon different CNT contents in the composites, three different samples that contain 10, 20, and 30 wt % MWCNT respectively (determined by TGA data given in Supporting Information Figure S1) were prepared and tested for charge/discharge voltage profiles (see Figure S4 in the Supporting Information). The results confirmed that with the optimum MWCNT content of 20 wt %, we observed the best electrochemical performance. This result can be explained in the following. First, with a lower content of MWCNTs in composite, the connection between mesoporous TiO_2 spheres becomes poorer, resulting in the poor conductivity, and the contribution of MWCNTs to the lithium ion storage capacity and the rate capacity becomes less important as well. On the other hand, if the concentration of MWCNTs is too high (i.e., ∼30 wt %), MWCNTs are more likely to aggregate and block the open channels for lithium intercalation in mesoporous TiO_2 spheres, resulting in deterioration of the battery performance. Moreover, to investigate the role of MWCNTs in the composite, there is another set of three samples: (i) MTO/MWCNT that contains the optimum content of 20 wt % MWCNT, (ii) the MTO with MWCNTs by physical mixing (MTO + MWCNT), and (iii) the MTO with carbon black (MTO + C) of the same carbon content with that of MTO/MWCNT composite; see Figure S5 in the Supporting Information). The result indicated that MTO/MWCNT composites exhibited the best performance.

A good electrical conductivity and mesoporosity of a structure is known to contribute to a high charge/discharge rate performance.[43] Figure 7b shows the impedance plots for commercial TiO_2, mesoporous TiO_2 spheres, and MTO/MWCNT composite electrodes after the first discharge−charge cycle. According to a previous report,[44] semicircular discharge/charge characteristics are related to the charge transfer through the electrode/electrolyte interface, and the steep increase in the line at a low frequency reflects the solid-state diffusion of the Li ions in the bulk materials. Figure 7b clearly shows that the size of the semicircle for the MTO/MWCNT composite was much smaller than that of commercial TiO_2 or mesoporous TiO_2 spheres. This implies that CNTs play an important role in improving the conductivity of the composite, leading to an improvement in the rate capability of the electrode.

The practical use of batteries depends on the electrochemical stability, and thus, the stability and reproducibility of the prepared electrodes is tested by observing the cyclic behaviors of these different samples at a rate of 1C, as shown in Figure 7c.

DOI: 10.1021/am508158v
ACS Appl. Mater. Interfaces 2015, 7, 3676−3683

The discharge capacity of the MTO/MWCNT composite during the first cycle was 269 mA h g^{-1} at 1C, and we observed a 3.1% decrease in capacity after 100 cycles. However, the mesoporous TiO_2 and the commercial TiO_2 exhibited corresponding values of 233 mA h g^{-1} with a 6.5% loss and 179 mA h g^{-1} with a 17.7% loss, respectively. Thus, the MTO/MWCNT anode is far superior to conventional TiO_2 anodes, which typically shows loss in the capacity greater than 20% after 1000 cycles. Since the loss in the capacity is mainly caused by Li^+ ions trapped in the anatase framework,[10−12] our results suggest that the MTO/MWCNT composite is an ideal structure that can inhibit Li^+ ion trapping. Moreover, the MTO/MWCNT composite anode is also superior to other TiO_2-based anodes, such as TiO_2−graphene−CNT nanocomposites (capacity loss of 8.7%).[41] The Coulombic efficiency of the synthesized structures was found to be nearly 100% for each cycle, indicating highly stable and reversible charge−discharge behavior at 1C. Therefore, the corresponding Coulombic efficiencies for the commercial TiO_2 and mesoporous TiO_2 spheres were of 95% and 97%, respectively.

4. CONCLUSION

In summary, we have synthesized highly stable TiO_2/MWCNT hybrid mesoporous material for use as an anode with a high specific capacity and superior rate capability. A simple two-step method was used combining sol−gel and solvothermal processes. The composite demonstrated excellent LIB performance with a discharge capacity as high as 316 mA h g^{-1}, as well as an excellent reversibility and stability after 100 cycles. We believe that the significant improvement in the LIB performance of the mesoporous TiO_2/MWCNT based composite is a result of the following features of the carefully designed structure. First, the MWCNTs served as conducting channels that connected each of the mesoporous TiO_2 spheres to efficiently transport electrons. Second, the mesoporous nature of the composite offered more open channels for Li^+ ion insertion/extraction while the thin walls of the mesoporous TiO_2 reduced the Li ion diffusion length in the solid phase while the pores allowed Li^+ ions to flow smoothly. Thus, the CNT interconnections and the porous structure of composite are expected to significantly improve battery performance.

■ ASSOCIATED CONTENT

Supporting Information

Additional cyclic voltammograms and charge/discharge profiles for commercial TiO_2 and mesoporous TiO_2. This material is available free of charge via the Internet at http://pubs.acs.org.

■ AUTHOR INFORMATION

Corresponding Author

*Tel.: +82-31-290-5906. Fax: +82-31-290-5947. E-mail: djkang@skku.edu.

Author Contributions

§Both authors contributed equally to this work.

Notes

The authors declare no competing financial interest.

■ ACKNOWLEDGMENTS

This work was supported by the Center for BioNano Health-Guard funded by the Ministry of Science, ICT and Future Planning (MSIP) of Korea as part of the Global Frontier Project (HGUARD_2013M3A6B2078944). We would also like to acknowledge the financial support by Fundamental Technology Research Program through the National Research Foundation of Korea (NRF) grants funded by Korean government (MSIP) (2014M3A7B4052201).

■ REFERENCES

(1) Tarascon, J. M.; Armand, M. Issues and Challenges Facing Rechargeable Lithium Batteries. *Nature* **2001**, *414*, 359−367.
(2) Kang, K.; Meng, Y. S.; Bréger, J.; Grey, C. P.; Ceder, G. Electrodes with High Power and High Capacity for Rechargeable Lithium Batteries. *Science* **2006**, *311*, 977−980.
(3) Goodenough, J. B.; Kim, Y. Challenges for Rechargeable Li Batteries. *Chem. Mater.* **2009**, *22*, 587−603.
(4) Marom, R.; Amalraj, S. F.; Leifer, N.; Jacob, D.; Aurbach, D. A Review of Advanced and Practical Lithium Battery Materials. *J. Mater. Chem.* **2011**, *21*, 9938−9954.
(5) Sun, Z.; Kim, J. H.; Zhao, Y.; Bijarbooneh, F.; Malgras, V.; Lee, Y.; Kang, Y.-M.; Dou, S. X. Rational Design of 3D Dendritic TiO_2 Nanostructures with Favorable Architectures. *J. Am. Chem. Soc.* **2011**, *133*, 19314−19317.
(6) Deng, D.; Kim, M. G.; Lee, J. Y.; Cho, J. Green Energy Storage Materials: Nanostructured TiO_2 and Sn-based Anodes for Lithium-ion Batteries. *Energy Environ. Sci.* **2009**, *2*, 818−837.
(7) Yang, Z.; Choi, D.; Kerisit, S.; Rosso, K. M.; Wang, D.; Zhang, J.; Graff, G.; Liu, J. Nanostructures and Lithium Electrochemical Reactivity of Lithium Titanites and Titanium Oxides: A review. *J. Power Sources* **2009**, *192*, 588−598.
(8) Nuspl, G.; Yoshizawa, K.; Yamabe, T. Lithium Intercalation in TiO_2 Modifications. *J. Mater. Chem.* **1997**, *7*, 2529−2536.
(9) Wagemaker, M.; van de Krol, R.; Kentgens, A. P. M.; van Well, A. A.; Mulder, F. M. Two Phase Morphology Limits Lithium Diffusion in TiO_2 (Anatase): A 7Li MAS NMR Study. *J. Am. Chem. Soc.* **2001**, *123*, 11454−11461.
(10) Chen, J. S.; Lou, X. W. Anatase TiO_2 Nanosheet: An Ideal Host Structure for Fast and Efficient Lithium Insertion/Extraction. *Electrochem. Commun.* **2009**, *11*, 2332−2335.
(11) Chen, J. S.; Tan, Y. L.; Li, C. M.; Cheah, Y. L.; Luan, D.; Madhavi, S.; Boey, F. Y. C.; Archer, L. A.; Lou, X. W. Constructing Hierarchical Spheres from Large Ultrathin Anatase TiO_2 Nanosheets with Nearly 100% Exposed (001) Facets for Fast Reversible Lithium Storage. *J. Am. Chem. Soc.* **2010**, *132*, 6124−6130.
(12) Das, S. K.; Darmakolla, S.; Bhattacharyya, A. J. High Lithium Storage in Micrometre Sized Mesoporous Spherical Self-assembly of Anatase Titania Nanospheres and Carbon. *J. Mater. Chem.* **2010**, *20*, 1600−1606.
(13) Jiang, C.; Wei, M.; Qi, Z.; Kudo, T.; Honma, I.; Zhou, H. Particle Size Dependence of the Llithium Storage Capability and High Rate Performance of Nanocrystalline Anatase TiO_2 Electrode. *J. Power Sources* **2007**, *166*, 239−243.
(14) Wang, K.; Wei, M.; Morris, M. A.; Zhou, H.; Holmes, J. D. Mesoporous Titania Nanotubes: Their Preparation and Application as Electrode Materials for Rechargeable Lithium Batteries. *Adv. Mater.* **2007**, *19*, 3016−3020.
(15) Yue, W.; Randorn, C.; Attidekou, P. S.; Su, Z.; Irvine, J. T. S.; Zhou, W. Syntheses, Li Insertion, and Photoactivity of Mesoporous Crystalline TiO_2. *Adv. Funct. Mater.* **2009**, *19*, 2826−2833.
(16) Guo, Y.-G.; Hu, Y.-S.; Maier, J. Synthesis of Hierarchically Mesoporous Anatase Spheres and their Application in Lithium Batteries. *Chem. Commun.* **2006**, *26*, 2783−2785.
(17) Liu, H.; Bi, Z.; Sun, X.-G.; Unocic, R. R.; Paranthaman, M. P.; Dai, S.; Brown, G. M. Mesoporous TiO2−B Microspheres with Superior Rate Performance for Lithium Ion Batteries. *Adv. Mater.* **2011**, *23*, 3450−3454.
(18) Huang, B.; Zheng, X.; Jia, D.; Lu, M. Design and Synthesis of High-rate Micron-sized, Spherical LiFePO4/C Composites Containing Clusters of Nano/microspheres. *Electrochim. Acta* **2010**, *55*, 1227−1231.

DOI: 10.1021/am508158v
ACS Appl. Mater. Interfaces 2015, 7, 3676−3683

(19) Guo, Y. G.; Hu, Y. S.; Sigle, W.; Maier, J. Superior Electrode Performance of Nanostructured Mesoporous TiO_2 (Anatase) through Efficient Hierarchical Mixed Conducting Networks. *Adv. Mater.* **2007**, *19*, 2087−2091.
(20) Moriguchi, I.; Hidaka, R.; Yamada, H.; Kudo, T.; Murakami, H.; Nakashima, N. A Mesoporous Nanocomposite of TiO_2 and Carbon Nanotubes as a High-Rate Li-Intercalation Electrode Material. *Adv. Mater.* **2006**, *18*, 69−73.
(21) Cao, F.-F.; Guo, Y.-G.; Zheng, S.-F.; Wu, X.-L.; Jiang, L.-Y.; Bi, R.-R.; Wan, L.-J.; Maier, J. Symbiotic Coaxial Nanocables: Facile Synthesis and an Efficient and Elegant Morphological Solution to the Lithium Storage Problem. *Chem. Mater.* **2010**, *22*, 1908−1914.
(22) Wang, D.; Choi, D.; Li, J.; Yang, Z.; Nie, Z.; Kou, R.; Hu, D.; Wang, C.; Saraf, L. V.; Zhang, J.; Aksay, I. A.; Liu, J. Self-Assembled TiO_2−Graphene Hybrid Nanostructures for Enhanced Li-Ion Insertion. *ACS Nano* **2009**, *3*, 907−914.
(23) Chen, J. S.; Wang, Z.; Dong, X. C.; Chen, P.; Lou, X. W. Graphene-wrapped TiO_2 Hollow Structures with Enhanced Lithium Storage Capabilities. *Nanoscale* **2011**, *3*, 2158−2161.
(24) Park, S.-J.; Kim, H.; Kim, Y.-J.; Lee, H. Preparation of Carbon-coated TiO_2 Nanostructures for Lithium-ion Batteries. *Electrochim. Acta* **2011**, *56*, 5355−5362.
(25) Park, S.-J.; Kim, Y.-J.; Lee, H. Synthesis of Carbon-coated TiO_2 Nanotubes for High-power Lithium-ion Batteries. *J. Power Sources* **2011**, *196*, 5133−5137.
(26) Cui, L.-F.; Hu, L.; Choi, J. W.; Cui, Y. Light-Weight Free-Standing Carbon Nanotube-Silicon Films for Anodes of Lithium Ion Batteries. *ACS Nano* **2010**, *4*, 3671−3678.
(27) Ding, S.; Chen, J. S.; Lou, X. W. One-Dimensional Hierarchical Structures Composed of Novel Metal Oxide Nanosheets on a Carbon Nanotube Backbone and Their Lithium-Storage Properties. *Adv. Funct. Mater.* **2011**, *21*, 4120−4125.
(28) Eder, D.; Windle, A. H. Carbon−Inorganic Hybrid Materials: The Carbon-Nanotube/TiO_2 Interface. *Adv. Mater.* **2008**, *20*, 1787−1793.
(29) Eder, D.; Windle, A. H. Morphology Control of CNT-TiO_2 Hybrid Materials and Rutile Nanotubes. *J. Mater. Chem.* **2008**, *18*, 2036−2043.
(30) Eder, D. Carbon Nanotube−Inorganic Hybrids. *Chem. Rev.* **2010**, *110*, 1348−1385.
(31) Huang, H.; Zhang, W. K.; Gan, X. P.; Wang, C.; Zhang, L. Electrochemical Investigation of TiO_2/carbon Nanotubes Nanocomposite as Anode Materials for Lithium-ion Batteries. *Mater. Lett.* **2007**, *61*, 296−299.
(32) Wen, Z.; Ci, S.; Mao, S.; Cui, S.; Lu, G.; Yu, K.; Luo, S.; He, Z.; Chen, J. TiO_2 Nanoparticles-decorated Carbon Nanotubes for Significantly Improved Bioelectricity Generation in Microbial Fuel Cells. *J. Power Sources* **2013**, *234*, 100−106.
(33) Tsai, M.-C.; Tsai, T.-L.; Shieh, D.-B.; Chiu, H.-T.; Lee, C.-Y. Detecting HER2 on Cancer Cells by TiO_2 Spheres Mie Scattering. *Anal. Chem.* **2009**, *81*, 7590−7596.
(34) Cooke, D. J.; Eder, D.; Elliott, J. A. Role of Benzyl Alcohol in Controlling the Growth of TiO_2 on Carbon Nanotubes. *J. Phys. Chem. C* **2010**, *114*, 2462−2470.
(35) Yin, Y.; Hu, Y.; Wu, P.; Zhang, H.; Cai, C. A Graphene-amorphous $FePO_4$ Hollow Nanosphere Hybrid as a Cathode Material for Lithium ion Batteries. *Chem. Commun.* **2012**, *48*, 2137−2139.
(36) Li, N.; Liu, G.; Zhen, C.; Li, F.; Zhang, L.; Cheng, H.-M. Battery Performance and Photocatalytic Activity of Mesoporous Anatase TiO_2 Nanospheres/Graphene Composites by Template-Free Self-Assembly. *Adv. Funct. Mater.* **2011**, *21*, 1717−1722.
(37) Sing, K. S. W.; Everett, D. H.; Haul, R. A. W.; Moscou, L.; Pierotti, R. A.; Rouquerol, J.; Siemieniewska, T. Reporting Physisorption Data for Gas/Solid Systems, with Special Reference to the Determination of Surface Area and Porosity. *Pure Appl. Chem.* **1985**, *57*, 603−619.
(38) Lindström, H.; Södergren, S.; Solbrand, A.; Rensmo, H.; Hjelm, J.; Hagfeldt, A.; Lindquist, S.-E. Li^+ Ion Insertion in TiO_2 (Anatase). 2. Voltammetry on Nanoporous Films. *J. Phys. Chem. B* **1997**, *101*, 7717−7722.
(39) Sudant, G.; Baudrin, E.; Larcher, D.; Tarascon, J.-M. Electrochemical Lithium Reactivity with Nanotextured Anatase-type TiO_2. *J. Mater. Chem.* **2005**, *15*, 1263−1269.
(40) Saravanan, K.; Ananthanarayanan, K.; Balaya, P. Mesoporous TiO_2 with High Packing Density for Superior Lithium Storage. *Energy Environ. Sci.* **2010**, *3*, 939−948.
(41) Shen, L.; Zhang, X.; Li, H.; Yuan, C.; Cao, G. Design and Tailoring of a Three-Dimensional TiO_2−Graphene−Carbon Nanotube Nanocomposite for Fast Lithium Storage. *J. Phys. Chem. Lett.* **2011**, *2*, 3096−3101.
(42) Ding, S.; Chen, J. S.; Luan, D.; Boey, F. Y. C.; Madhavi, S.; Lou, X. W. Graphene Supported Anatase TiO_2 Nanosheets for Fast Lithium Storage. *Chem. Commun.* **2011**, *47*, 5780−5782.
(43) Wang, B.; Xin, H.; Li, X.; Cheng, J.; Yang, G.; Nie, F., Mesoporous CNT@TiO_2-C Nanocable with Extremely Durable High Rate Capability for Lithium-Ion Battery Anodes. *Sci. Rep.* **2014**, *4*.
(44) Xie, J.; Zhao, X. B.; Cao, G. S.; Zhao, M. J. Electrochemical Performance of $CoSb_3$/MWNTs Nanocomposite Prepared by In-situ Solvothermal Synthesis. *Electrochim. Acta* **2005**, *50*, 2725−2731.

DOI: 10.1021/am508158v
ACS Appl. Mater. Interfaces 2015, 7, 3676−3683